

F_γ : a new observable for photon-hadron discrimination in hybrid air shower events

M. Niechciol^{a,*}, M. Risse^a, P. Ruehl^a, M. Settimo^{a,b,1}, P. W. Young^{a,2}, A. Yushkov^{a,c,3}

^a*Universität Siegen, Department Physik, Siegen, Germany*

^b*Laboratoire de Physique Nucléaire et de Hautes Energies (LPNHE), Universités Paris 6 et Paris 7, CNRS-IN2P3, Paris, France*

^c*Instituto de Tecnologías en Detección y Astropartículas (CNEA, CONICET, UNSAM), Buenos Aires, Argentina*

Abstract

To search for ultra-high-energy photons in primary cosmic rays, air shower observables are needed that allow a good separation between primary photons and primary hadrons. We present a new observable, F_γ , which can be extracted from ground-array data in hybrid events, where simultaneous measurements of the longitudinal and the lateral shower profile are performed. The observable is based on a template fit to the lateral distribution measured by the ground array with the template taking into account the complementary information from the measurement of the longitudinal profile, i.e. the primary energy and the geometry of the shower. F_γ shows a very good photon-hadron separation, which is even superior to the separation given by the well-known X_{\max} observable (the atmospheric depth of the shower maximum). At energies around 1 EeV (10 EeV), F_γ provides a background rejection better than 97.8% (99.9%) at a signal efficiency of 50%. Advantages of the observable F_γ are its technical stability with respect to irregularities in the ground array (i.e. missing or temporarily non-operating stations) and that it can be applied over the full energy range accessible to the air shower detector, down to its threshold energy. Furthermore, F_γ complements nicely to X_{\max} such that both observables can well be combined to achieve an even better discrimination power, exploiting the rich information available in hybrid events.

Keywords: Photons, Cosmic Rays, Hybrid Detector, Lateral Distribution Function, LDF

1. Introduction

The discovery of ultra-high-energy (UHE) photons, i.e. photons with an energy larger than $\sim 10^{18}$ eV = 1 EeV, in primary cosmic rays would be of particular interest not only for the field of astroparticle physics, but also for related fields such as particle physics, astrophysics and fundamental physics [1]. For example, UHE photons are tracers of the Greisen-Zatsepin-Kuzmin (GZK) process, i.e. the interactions of UHE protons, propagating through the Universe, with photons from the cosmic microwave background (CMB). In these interactions, neutral pions are produced via the Delta resonance ($p + \gamma_{\text{CMB}} \rightarrow \Delta^+ \rightarrow p + \pi^0$). These pions subsequently decay into pairs of UHE photons with energies at typically 10% of the energy of the primary UHE proton. If these predicted GZK photons are observed on Earth, it would be an indicator for the GZK process being the reason for the observed suppression in the energy spectrum of UHE cosmic rays (UHECR) [2].

Observing UHE photons could also help to pinpoint the very sources of UHECR, since photons, unlike charged cosmic rays, are not deflected by magnetic fields. The attenuation length for photons in the EeV range varies between some 100 kpc at 1 EeV and a few Mpc at 10 EeV [3], encompassing possible galactic and nearby extragalactic sources. The detection of UHE photons is of great interest for fundamental physics as well. For instance, the registration of a single photon in the EeV range could improve existing bounds on Lorentz invariance violation in the context of a modified Maxwell theory by several orders of magnitude [4]. In addition, observing the particle cascade initiated by a UHE photon in the atmosphere allows testing particle interactions at extreme energies and searching for new physics [1, 5].

Due to their small incoming flux (less than one particle per square kilometer per year), UHE cosmic particles impinging on the Earth can only be detected indirectly through the measurement of the air showers they initiate when entering the Earth's atmosphere. For the identification of primary photons in the recorded air shower data, the challenge is to separate photon-induced showers from those initiated by hadrons. Thus, the differences between these two classes of air showers are of great importance. Air showers initiated by UHE photons develop, on average, deeper in the atmosphere than air showers of the

*Corresponding author

Email address: niechciol@physik.uni-siegen.de (M. Niechciol)

¹Now at SUBATECH, CNRS/IN2P3, Université de Nantes, École des Mines de Nantes, Nantes, France

²Now at Physics Division, Los Alamos National Laboratory, Los Alamos, NM, USA

³Now at Institute of Physics (FZU) of the Academy of Sciences of the Czech Republic, Prague, Czech Republic

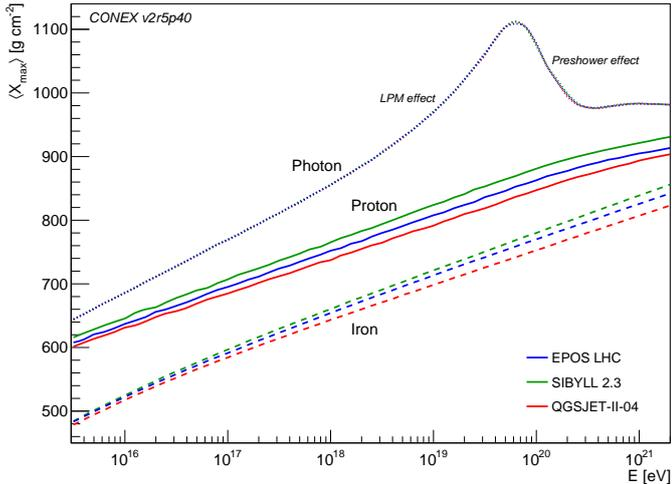


Figure 1: Average atmospheric depth of the shower maximum, $\langle X_{\max} \rangle$, as a function of the primary energy for simulated air showers initiated by photons, protons and iron nuclei. The simulations have been done using the Conex simulation code [6, 7] with three different hadronic interaction models (EPOS LHC [8], SIBYLL 2.3 [9, 10] and QGSJET-II-04 [11]). For the calculation of the preshower effect, the location of the Pierre Auger Observatory in Argentina has been used.

same primary energy initiated by hadrons. This can be expressed through the observable X_{\max} , which describes the atmospheric depth of the shower maximum (see Fig. 1). At larger energies, additional effects like the Landau-Pomeranchuk-Migdal (LPM) effect and preshower processes above the atmosphere, which further influence the shower development, have to be taken into account [1]. X_{\max} has become a key observable for current cosmic-ray research, mostly due to the fact that it can be accessed directly using the air-fluorescence technique. Current air shower experiments like the Pierre Auger Observatory [12] or the Telescope Array [13] are following a hybrid approach, where fluorescence detectors are complemented by a ground array of particle detectors. The typical X_{\max} resolution of e.g. the Pierre Auger Observatory is better than 26 g cm^{-2} at energies around $10^{17.8} \text{ eV}$, improving with energy to about 15 g cm^{-2} above $10^{19.3} \text{ eV}$ [14]. This is much smaller than the differences in the average X_{\max} between photon- and hadron-induced air showers at these energies ($\sim 100 \text{ g cm}^{-2}$ at 10^{18} eV and $\sim 160 \text{ g cm}^{-2}$ at 10^{19} eV , cf. Fig. 1).

To fully exploit this hybrid approach and to improve the photon-hadron separation power, it is useful to complement the observable X_{\max} with an additional observable that is based on the data from the ground array. In the past, observables such as the curvature of the shower front or the risetime of the signals in the detectors of the ground array have been used in the context of the search for photons [15, 16]. However, such observables can only be reliably estimated when a minimum number of detectors of the ground array have triggered. For example, at least five detectors are needed to determine the curvature

of the shower front with acceptable accuracy. This effectively places a lower limit—for past analyses typically at 10 EeV —on the energy region that can be accessed with an analysis based on these observables. At lower energies, i.e. in the EeV range, the observable S_b [17] has been successfully used in past analyses [18, 19, 20, 3]. S_b is based on the sum of the signals S_i , measured in the individual detectors i of the ground array, weighted by the distances r_i of the detectors to the shower axis:

$$S_b = \sum_i S_i \left(\frac{r_i}{1000 \text{ m}} \right)^b, \quad (1)$$

with the free parameter b , which has to be fixed for a given analysis [21].

Air showers initiated by photons have, on average, a smaller S_b than air showers induced by hadrons of the same primary energy [21]. However, an observable like S_b can be significantly affected by any incompleteness in the detector array, which would lead to an underestimation of the true value. Such an incompleteness may be due to the borders of the array, due to missing detectors (important e.g. during the deployment phase of the array), or due to temporarily non-operating detectors. As an example for the latter effect, let us assume that at any time, 1% of the detectors from the ground array are temporarily non-operating. For an array geometry where the detectors are arranged on a hexagonal grid, this means that 6% of all events contain at least one non-operating detector in the first hexagon around the detector measuring the largest signal. When also the second hexagon is considered, about 18% of all measured events are affected. Special care must then be taken, e.g. in the event selection, to prevent an underestimation of the S_b value for a given event due to these incompletenesses, which could mimic the expected behaviour of a photon-induced air shower. This holds especially at energies not far from the energy threshold of the experiment, where usually only very few detectors of the ground array are triggered and an omission of a signal from a detector can alter the S_b value substantially.

In this paper, we describe a new observable, called F_γ , which can be used at all energies down to the threshold set by the shower array. This observable exploits, similarly to S_b , the lateral distribution of the density of secondary particles from the air shower on ground level and is, as will be discussed later, complementary to X_{\max} . Unlike S_b , missing stations will not alter the central value of F_γ (but only increase its uncertainty), leading to an improved stability of the observable. The lateral distribution can be described by a lateral distribution function (LDF), which can be determined from the ground-array data. The shape of the LDF depends on the type of the primary particle initiating the air shower: for photon-induced air showers, which on average exhibit a smaller number of secondary muons and a larger X_{\max} compared to hadron-induced air showers of the same primary energy, the LDF is steeper, leading

to a smaller signal in the detectors of the ground array compared to the signal measured from hadron-induced air showers at the same distance from the shower core. F_γ is based on a fit of the LDF. Therefore, it is largely unaffected by incompleteness of the ground array. In addition, F_γ can be determined for events with very few triggered detectors in the ground array (even just a single one), hence it can be applied also to lower-energy events, where observables such as the curvature of the shower front cannot be determined.

In the following sections, we describe how the observable F_γ is defined and evaluate the performance of the observable in distinguishing photon-induced air showers from those induced by hadrons by using Monte Carlo (MC) simulations of air showers.

2. Description of the observable

2.1. General idea

The observable F_γ is based on a template fit of an LDF to the data recorded by the ground array. In this fit, we assume the primary particle initiating the air shower was a photon, and we determine the expected signal recorded in a detector of the ground array at a reference distance under this assumption. In this fit, two things will be different between photon- and hadron-induced showers with the same primary energy. First, the LDF fit will better describe the lateral particle distributions for primary photons than for primary hadrons. Second, the signal at a certain distance from the shower core will be smaller for showers initiated by photons than for those initiated by hadrons, as is known from air shower physics. We exploit the second difference. We normalize the expected signal obtained from the fit to the average signal expected for hadron-induced air showers of the same primary energy and zenith angle, and we call the resulting quantity F_γ . In short, the sequence to determine F_γ for a given air shower event is as follows:

- From hybrid observations, in particular of the longitudinal shower profile, the energy E and zenith angle θ of the event are reconstructed;
- Using E and θ as an input, a photon LDF template is fit to the ground-array data of the event. The template is prepared in advance using extensive photon simulations. The fit determines the LDF normalization $S_{1000|\gamma}$, the only remaining free parameter of the template;
- The average ground signal $\langle S_{1000} \rangle$ in case of hadron-induced air showers expected for this event is calculated using E and θ . The relation between these quantities is known from the standard energy calibration of the ground array;
- F_γ for this event is then given by the ratio $\frac{S_{1000|\gamma}}{\langle S_{1000} \rangle}$.

2.2. Specific implementation

In the following section, we describe a specific realization of the observable F_γ . In particular, we use a given functional form to describe the LDF. However, the core concept of the observable as described above does not depend on the very choice of a functional form for the LDF or even a particular experimental setup, but it can be applied to different functional forms and adapted to different experiments.

To describe the LDF—i.e. the signal S measured in a detector at a perpendicular distance r from the shower axis—, we use an NKG-type function, which has the following form:

$$S(r) = k \left(\frac{r}{r_{\text{opt}}} \right)^\beta \left(\frac{r + r_s}{r_{\text{opt}} + r_s} \right)^\beta, \quad (2)$$

where r_{opt} is the optimum distance at which the characteristic parameters of the air shower can be determined to reduce e.g. uncertainties due to a lack of knowledge about the true LDF, r_s is a scaling parameter, k is a normalization parameter equal to the signal at the optimum distance, and β is the slope of the LDF. The choice of the optimum distance depends on the geometrical properties of the ground array. For the experimental setup of the Pierre Auger Observatory—which is assumed from now on—with its hexagonal grid and a spacing of 1500 m between the individual detectors, $r_{\text{opt}} \simeq 1000$ m is found [22]. The normalization parameter k is then commonly referred to as S_{1000} —and given in units of vertical equivalent muon (VEM)—, and the scaling parameter r_s is chosen as $r_s = 700$ m. The determination of the LDF is thus reduced to determining S_{1000} and β .

When only data from the ground array are available, the normalization parameter S_{1000} is used to estimate the energy of the primary particle initiating the recorded air shower. In hybrid events, however, the primary energy as well as other shower parameters such as the shower geometry can be determined from the data recorded by the fluorescence detectors. With this knowledge, we can introduce the template, or “photon-optimized”, fit of the LDF, which is the basis for the observable F_γ . In this fit, we fix the slope parameter β to the average value expected for a photon-induced air shower that has the same primary energy E and the same zenith angle θ as reconstructed from the fluorescence detector data. In general, the type of the primary particle that initiated the recorded air shower is not known. Hence, we use the photon energy E_γ , i.e. the calorimetric energy determined from the fluorescence detector data corrected for the missing energy expected for a photon-induced air shower (about 1% of the calorimetric energy [23]) as reference energy for all events in the application of the observable. Since the slope of the LDF is fixed in the photon-optimized LDF fit, only the normalization parameter, which we denote as $S_{1000|\gamma}$, has to be

determined from the fit. The function that is fitted to the data from the ground array thus reads

$$S(r) = S_{1000|\gamma} \left(\frac{r}{1000 \text{ m}} \right)^{\beta(E_\gamma, \theta)} \left(\frac{r + 700 \text{ m}}{1700 \text{ m}} \right)^{\beta(E_\gamma, \theta)}. \quad (3)$$

Since only a single parameter of the LDF has to be determined, the photon-optimized fit can also be applied to lower-energy events in the EeV range, where perhaps even only one detector from the ground array is triggered. On a technical note, we use a maximum-likelihood method to determine the photon-optimized LDF, which enables us to use not only the information from the triggered detectors in the fit, but also from non-triggering but active detectors. These effectively place an upper limit on the signal at the corresponding distance to the shower axis, and it is another advantage of the F_γ observable that this piece of information can be taken into account in a straightforward way.

To fix the slope parameter β , we use a phenomenological parameterization that has been derived from MC simulations of photon-induced air showers in the energy range between 1 and 10 EeV (referring to the true MC energy) and in the zenith angle range between 0 and 60°:

$$\beta(E_\gamma, \theta) = a_0(E_\gamma) + a_1(E_\gamma) (\sec(\theta) - 1)^3, \quad (4)$$

with

$$\begin{aligned} a_0(E_\gamma) &= b_0 + b_1 \log_{10}(E_\gamma [\text{eV}]), \\ a_1(E_\gamma) &= c_0 + c_1 \log_{10}(E_\gamma [\text{eV}]) + c_2 \log_{10}(E_\gamma [\text{eV}])^2. \end{aligned}$$

The five parameters b_0 , b_1 , c_0 , c_1 and c_2 are:

$$\begin{aligned} b_0 &= -0.695 \pm 0.098, \\ b_1 &= -0.107 \pm 0.005, \\ c_0 &= 506.72 \pm 0.11, \\ c_1 &= -53.159 \pm 0.006, \\ c_2 &= 1.3972 \pm 0.0003. \end{aligned}$$

In Fig. 2, the parameterized β , following Eq. 4, is given as a function of the energy E_γ for three different fixed zenith angles θ . Due to the dependence on secant cubed of the zenith angle, the curves for $\theta = 0^\circ$ and 30° are very similar. Only at larger zenith angles, the curves change significantly.

An example for the application of the photon-optimized fit to two simulated air shower events with the same MC energy and the same zenith angle—initiated by a primary photon and a primary proton, respectively—is shown in Fig. 3. As discussed before, the lateral distribution for the photon-induced air shower is steeper, leading to a smaller value of $S_{1000|\gamma}$. It should be pointed out here again that in the photon-optimized LDF template fit, β is fixed. Hence, the flatter LDF of a proton-induced air shower is not reproduced well. However, it is not the purpose of the fit

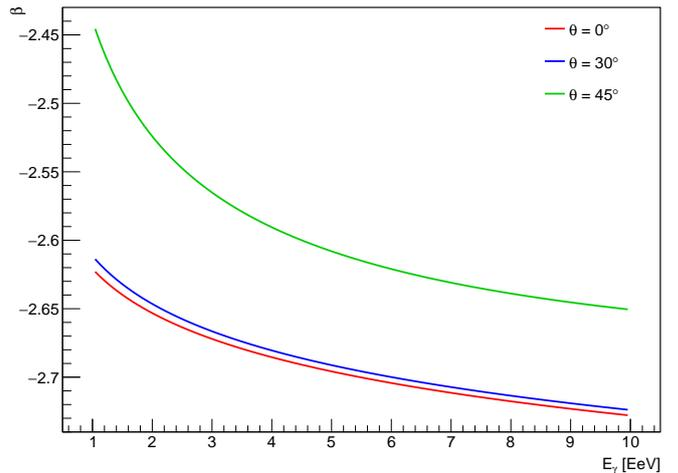


Figure 2: The parameterized slope parameter β (following Eq. 4) as a function of the photon energy E_γ for three different fixed zenith angles θ .

to reproduce the lateral distribution well and determine the “true” S_{1000} for any given event, but to provide a parameter that helps to discriminate photon-induced from hadron-induced air showers.

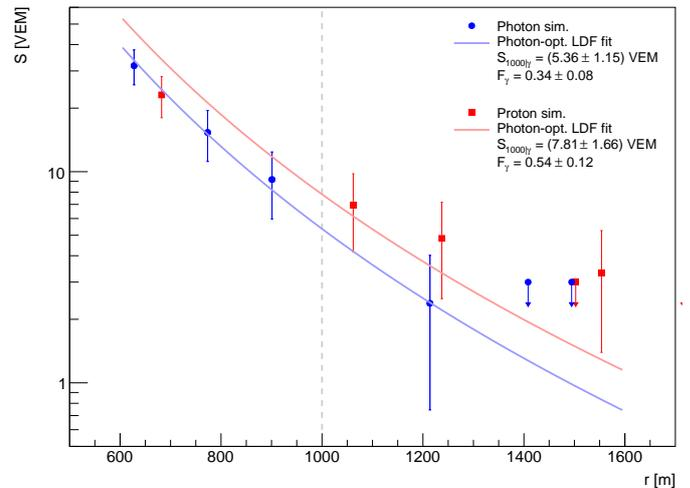


Figure 3: Example for the application of the photon-optimized fit of the LDF to two simulated air shower events with the same primary energy ($E_{MC} \sim 3.5$ EeV) and zenith angle ($\theta \sim 45^\circ$), but different primary particle types (photon in blue, proton in red). Non-triggering stations that are included in the photon-optimized LDF fit are indicated as upper limits (at 95% C.L.) on the expected signals at the corresponding distances.

The observable F_γ is eventually obtained by normalizing the $S_{1000|\gamma}$ that is determined from the photon-optimized fit to the value of S_{1000} that is expected for an average (hadron-induced) air shower with the same primary energy and the same zenith angle. Thus, F_γ is defined as

$$F_\gamma = \frac{S_{1000|\gamma}}{\langle S_{1000} \rangle (E_\gamma, \theta)}. \quad (5)$$

In hybrid events, the primary energy E and the zenith angle θ are determined from the data from the fluorescence detectors, hence $\langle S_{1000} \rangle$ can be calculated from the reconstructed energy and zenith angle by inverting the formulas for the energy calibration (for the dependence on the energy) and the Constant Intensity Cut (CIC) function (for the dependence on the zenith angle) [24]. As before, we use the photon energy E_γ for all events. For the two example events shown in Fig. 3, the F_γ values are 0.34 ± 0.08 for the photon event and 0.54 ± 0.12 for the proton event.

3. Performance

3.1. F_γ alone

To evaluate the performance of the observable for photon-hadron discrimination, a set of photon- and proton-induced air showers has been simulated with CORSIKA [25], version 7.4000, using QGSJET-II-04 [11] and Fluka2011.2b.6 [26, 27] as hadronic interaction models at high and low energies, respectively. In total, 20,000 air showers have been simulated in ten energy bins (equidistant in $\log_{10}(E_{MC})$) in the energy range between 1 and 10 EeV for each of the two primary particle types. As stated before, we use the setup of the Pierre Auger Observatory as an example for the application of the observable. Hence, we use the Offline software framework of the Auger collaboration [28] to simulate the detector response of the fluorescence detectors and the individual detectors of the ground array. For the air shower simulations, we use 10^{-6} optimum thinning [29, 30]. For the unthinning, we use the standard routines implemented in the Offline software framework, which are based on [31]. Each CORSIKA shower is re-sampled five times with the core position of the shower randomly distributed over the area of the ground array. The total data set of simulated air shower events contains 200,000 events. Several cuts are applied to the data set to ensure that only events of sufficient quality, i.e. with a well-reconstructed geometry and shower profile following the selection criteria from [20], enter the analysis. Overall, this event selection retains about 30% (43%) of all triggered photon (proton) events at energies around 1 EeV, increasing to 42% (69%) around 10 EeV. The differences between the selection efficiencies for primary photons and protons can be attributed to the differences between air showers initiated by the two particle types as discussed in Sec. 1.

In Fig. 4 (left column), the F_γ distributions for three different energy bins between $E_{MC} = 1$ EeV and $E_{MC} = 10$ EeV are shown. The average values of the distributions are roughly as expected from the definition of the observable (see Eq. 5): around 0.8 for the proton distributions (since $S_{1000|\gamma}$ from the photon-optimized LDF fit underestimates the “true” S_{1000} by construction, while $\langle S_{1000} \rangle(E_\gamma, \theta)$ is close to the “true” S_{1000}) and around 0.4 for the photon distributions ($S_{1000|\gamma}$ is, on average, close

to the “true” S_{1000} of photons, but $\langle S_{1000} \rangle(E_\gamma, \theta)$ is much larger than the “true” S_{1000}). Qualitatively, it can be seen that the distributions are well-separated. The separation gets larger with increasing energy. To quantify the separation between proton- and photon-induced air shower events, we use the merit factor η as a measure for the separation power of an observable. The merit factor is defined as

$$\eta = \frac{|\mu_\gamma - \mu_p|}{\sqrt{\sigma_\gamma^2 + \sigma_p^2}}, \quad (6)$$

with μ_γ and μ_p (σ_γ and σ_p) denoting the mean values (standard deviations) of the photon and proton distributions, respectively. For the case of the distributions shown in Fig. 4, merit factors of 1.40, 2.12 and 2.41 are obtained in the three different energy bins. The increase in the merit factor comes mostly from the smaller widths of the distributions at higher energies. With increasing energy, more stations are triggered and enter the LDF fit. Thus, fluctuations in the signals are mitigated in the fit, leading eventually to a narrower F_γ distribution. The mean values of the distributions do not change significantly. This is expected from the definition of the observable, since the energy dependence is largely removed by dividing $S_{1000|\gamma}$ by $\langle S_{1000} \rangle(E_\gamma, \theta)$.

For comparison, the merit factors of the corresponding X_{\max} distributions for the same data set have been calculated. Merit factors of 1.28, 1.76 and 1.97 have been obtained for the three energy bins. The merit factors calculated here are in good agreement with what is expected from parameterizations of the X_{\max} distributions for primary photons and protons at the corresponding energies [32]. For the same conditions, the separation power of F_γ in terms of η is thus larger than the separation power of the observable X_{\max} over the full energy range considered here. For the observable S_b with $b = 4$ —the value that has been used in [20]—a merit factor around 2 is found in [21] for energies averaged between $10^{18.5}$ eV and $10^{19.6}$ eV and a hexagonal grid with 1500 m spacing (cf. the merit factor of 2.41 for F_γ around 10^{19} eV). For other choices of b , the merit factor might be higher, but it should be noted that in [21], a semi-analytical approach was employed instead of a full MC simulation of the detector response. Overall, it can be stated that F_γ is at least on par with S_b in terms of the merit factor over the energy range considered here.

It should be noted however, that the merit factor takes into account only the mean and the width of the distributions and not the full shape. As an example, one could imagine a long tail in the proton distribution reaching beyond the bulk of the photon distribution. Proton events in this tail will very likely be misidentified as photon events, even though the bulk of the distributions may be well-separated, leading to a large merit factor. Hence, we employ a second measure for the separation power: the background rejection, i.e. the fraction of events in the proton

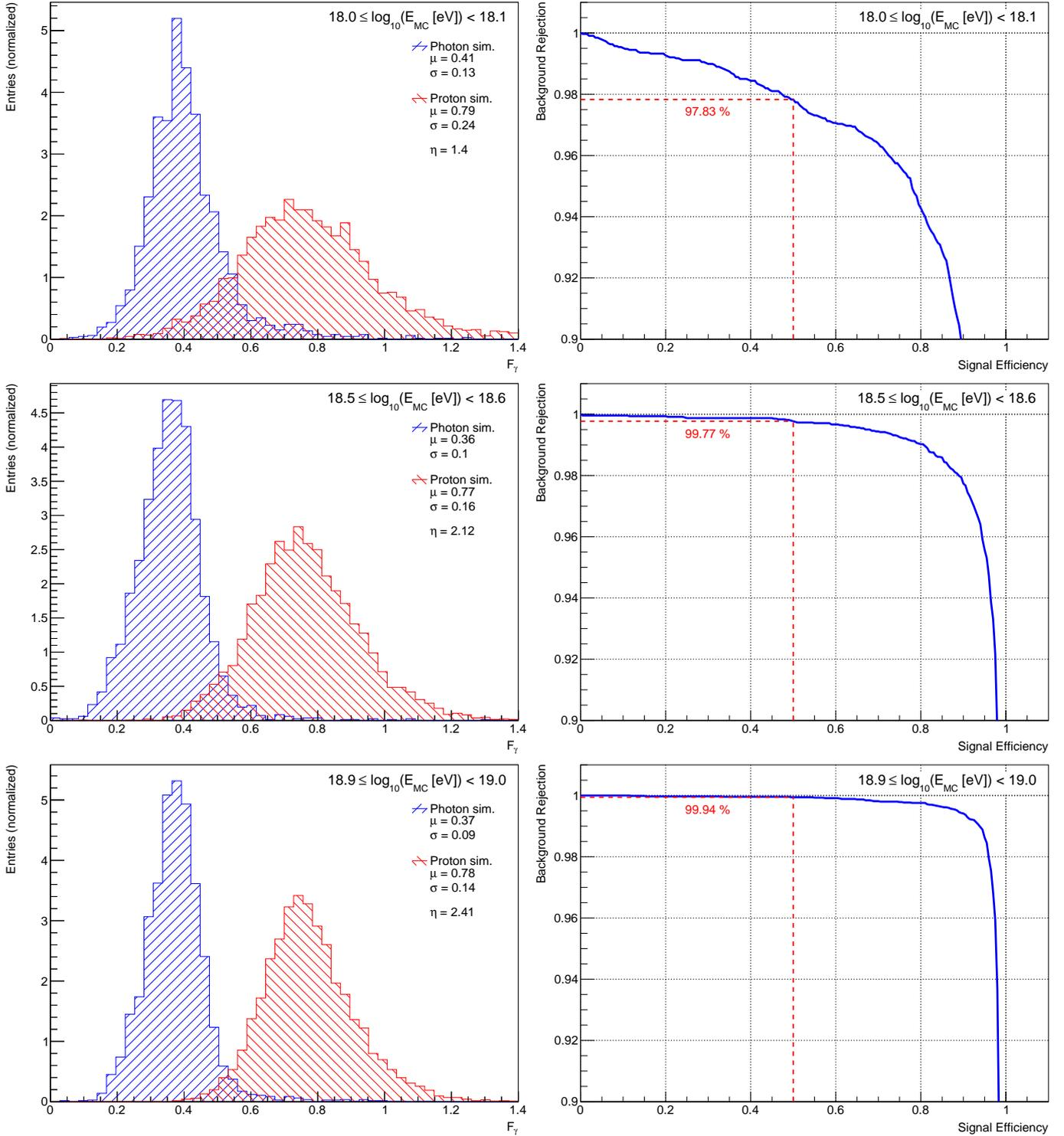


Figure 4: Performance of F_γ in three different energy bins between $E_{MC} = 1 \text{ EeV}$ and $E_{MC} = 10 \text{ EeV}$. Left column: distributions of F_γ for primary photons (blue) and protons (red). The mean values μ and the standard deviations σ of the distributions as well as the merit factors η calculated from these values are indicated in the plots. Right column: background rejection as a function of the signal efficiency, calculated from the F_γ distributions. The background rejection at a signal efficiency of 50% is indicated by the dashed red lines.

distribution rejected by a given cut value on the observable, as a function of the signal efficiency, i.e. the fraction of events in the photon distribution that pass the given cut. The resulting curves are shown in Fig. 4 (right column). As reference value for the separation power, the background rejection at a signal efficiency of 50 % (i.e. the cut value corresponds to the median of the photon distribution) is usually taken. From the three curves shown in Fig. 4, values of 97.83 %, 99.77 % and 99.94 % are obtained for the three energy bins. As before, the corresponding values for the observable X_{\max} have also been determined for comparison. In the three energy bins, values of 92.60 %, 97.57 % and 98.48 % were calculated.

In Fig. 5, the performance of the F_γ observable in comparison with X_{\max} is shown over the full energy range from 1 to 10 EeV. In terms of the merit factor, the separation power of both observables increases linearly with the logarithm of the energy, albeit with a larger slope for F_γ . In terms of the background rejection, both curves converge exponentially towards 100 %. However, the F_γ curve converges much faster: already around $10^{18.4}$ eV, the curve is above 99.5 %, while the X_{\max} curve is still below 98.5 % around 10^{19} eV.

3.2. Combination with X_{\max}

In a realistic application, F_γ will not be used as a stand-alone observable, but rather in combination with some other observable, e.g. X_{\max} , to fully exploit the information available in hybrid events. Hence, we will now discuss the potential performance of the combination of the two observables F_γ and X_{\max} . In Fig. 6, scatter plots of the two observables in three different energy bins are shown. Within the individual data sets, the two observables are largely uncorrelated, with the correlation coefficients close to zero. Comparing the photon and the proton data sets, it can be seen that the two observables complement each other well. The distributions are well separated in the (F_γ, X_{\max}) space, with the separation increasing with energy as before. Especially at higher energies, only very few proton events are found in the regions where the bulk of the photon distribution is located. Already by applying simple cuts on the two observables, it is possible to reach a background rejection very close to 100 % (i.e. comparable to the background rejection quoted above for F_γ), but at a much larger signal efficiency.

Another possibility is to combine the two observables in a Multi-Variate Analysis (MVA). To illustrate the potential of an MVA combining F_γ and X_{\max} , we use a simple linear Fisher discriminant analysis [34]. The Fisher analysis has the advantages that it can be calculated analytically and that it provides robust and very good event classification for uncorrelated input observables, as is the case for F_γ and X_{\max} . In Fig. 7, the distribution of the Fisher discriminant is shown exemplarily for the first energy bin. As expected from the scatter plots, the distributions are very

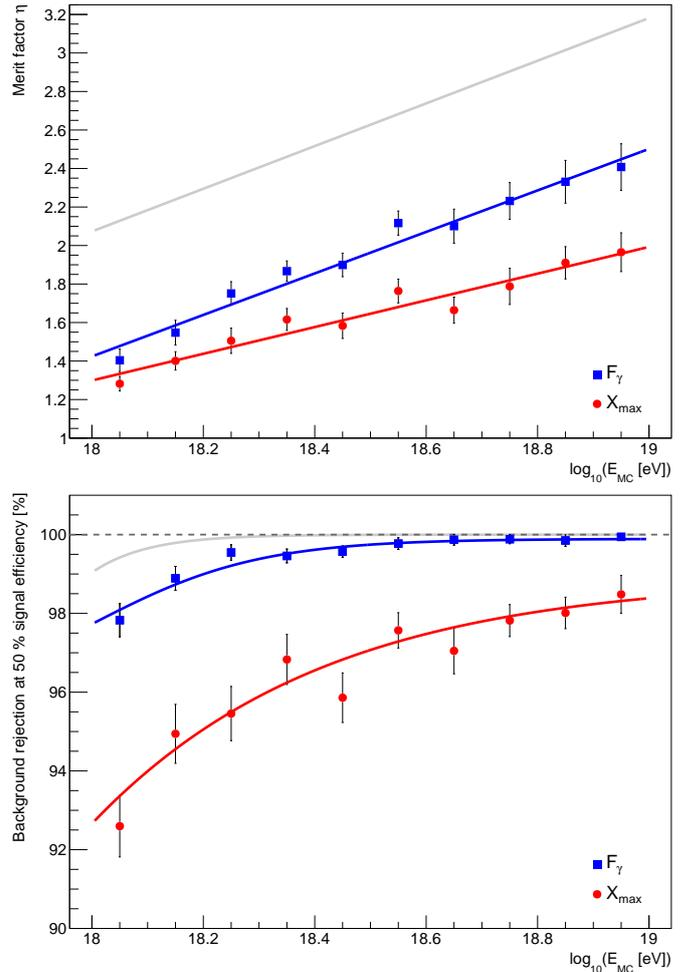


Figure 5: Separation power of F_γ (red) between $E_{MC} = 1$ EeV and $E_{MC} = 10$ EeV, compared to the separation power of X_{\max} (blue). Top: merit factor η ; bottom: background rejection ρ at 50 % signal efficiency. The uncertainties on η and ρ have been determined using the bootstrapping method [33]. The red and blue lines have been included to guide the eye, while the gray lines indicate the separation power of a possible combination of the two observables in a simple Fisher analysis (cf. Sec. 3.2).

well separated. The overlap between the photon and the proton distributions is smaller than for F_γ alone. Consequently, the merit factor increases to 2.0, while the background rejection at a signal efficiency of 50 % increases to 99.39 %. In other words, the combination of both observables can reduce the background contamination at this signal efficiency and in this energy bin by more than a factor of 3 compared to F_γ alone and more than a factor of 12 compared to X_{\max} alone. At higher energies, the combination of the two observables performs similarly well (see also Fig. 5). The merit factors increase to 2.82 and 3.10 in the second and third energy bin from Fig. 4, respectively. The values for the background rejection rise to 99.94 % in the second energy bin and 100 % (within the limited statistics available in the data sets used here) in the third energy bin.

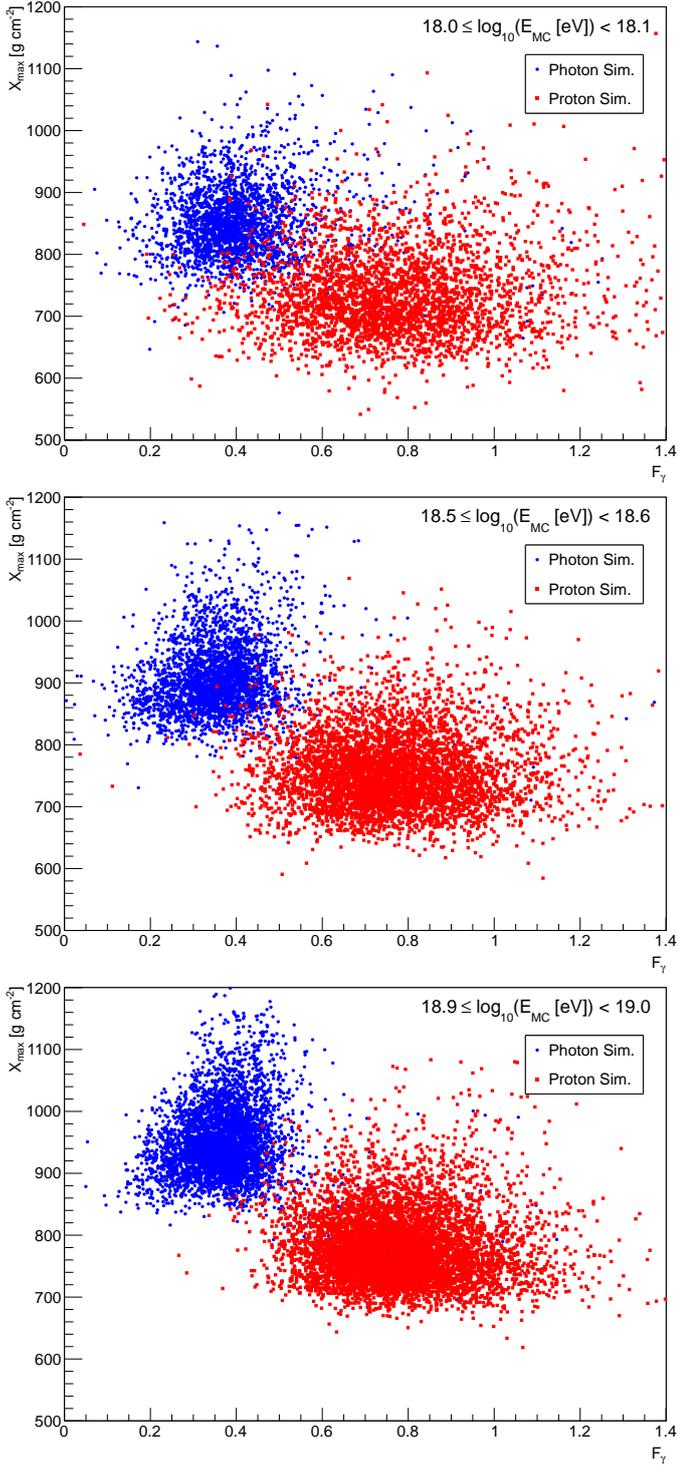


Figure 6: Scatter plots of F_γ and X_{\max} in three different energy bins between $E_{\text{MC}} = 1 \text{ EeV}$ and $E_{\text{MC}} = 10 \text{ EeV}$ for primary photons (blue) and protons (red).

4. Discussion

In summary, we introduced a new observable, called F_γ , to improve the photon-hadron separation in air shower events measured simultaneously by fluorescence detectors and a ground array. F_γ shows very good separation power

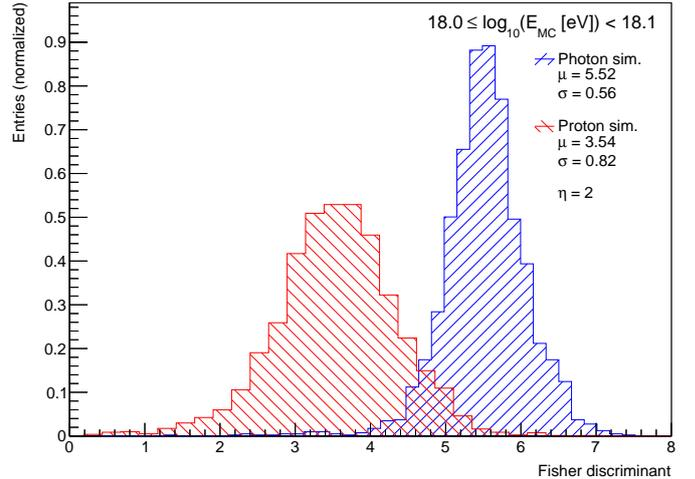


Figure 7: Example for the performance of a combination of F_γ and X_{\max} in an MVA: distribution of the Fisher discriminant in the first energy bin (cf. Fig. 4).

and complements nicely to X_{\max} . Combining both observables in an MVA leads to a background rejection of 99.39% at 50% signal efficiency at energies around 10^{18} eV , improving further with increasing energy. In other words, the observable allows one to reach a nearly background-free regime while still keeping a significant fraction of the signal. A particular advantage of F_γ is its reconstruction stability: it can be applied also at energies close to the energy threshold of the experiment, where perhaps even just a single detector from the ground array is triggered. The absence of a signal measured in an active station can be taken into account as well. In addition, the observable is not affected significantly by incompleteness of the ground array, e.g. at the borders of the array or due to temporarily non-operating detectors. We explicitly checked this by removing triggered stations from a (simulated) event and repeating the photon-optimized LDF fit without these stations. On average, the deviation of the resulting F_γ value from the one obtained with all stations included in the fit is in the order of a few percent only, which is within the average uncertainties on F_γ . Especially if only one or two stations are removed, the deviation is practically negligible. We also note that the observable is not significantly affected by uncertainties in the hadronic interaction models used in air shower simulations. This is because the template used in the photon-optimized LDF fit is based only on photon simulations, where the impact of the choice of the hadronic interaction model is practically negligible (cf. Fig. 1). The method of the LDF template fit can be easily adapted to other experimental setups than the case of the Pierre Auger Observatory discussed in this paper. This includes mixed configurations as well, where e.g. a part of the ground array has a denser arrangement of detectors.

In this work, we discussed the application of the F_γ ob-

servable for hybrid data, i.e. data where simultaneous measurements from both a fluorescence detector and a ground array are available. However, the observable is not limited to the particular combination of a fluorescence detector and a ground array. Only the reconstructed shower geometry and primary energy are needed in addition to the data from the ground array to determine F_γ . This additional information could also be obtained from e.g. radio measurements of air showers, which may start to develop into a viable possibility to measure the longitudinal development of air showers in the atmosphere without the limitations in detector uptime that the air-fluorescence techniques faces [35].

The method of the LDF template fit could also be applied to mass composition studies, since the characteristic differences between proton-induced and iron-induced air showers are similar to the differences between air showers initiated by photons and protons (i.e. larger X_{\max} , cf. Fig. 1, and smaller number of muons). A preliminary study of the proton-iron separation using F_γ without any changes to the observable compared to this work leads to merit factors comparable to those obtained with X_{\max} at energies around 10^{19} eV. In a real application, the template used in the LDF fit should be adapted, i.e. the fit should be optimized to e.g. primary iron nuclei. If the appropriate template is used, it can be expected that the performance of an F_γ -like observable for proton-iron separation is even higher.

So far, we used a basic event selection to ensure that only events of sufficient reconstruction quality enter the analysis. The overall photon-hadron separation could be improved further by introducing additional event selection criteria, optimized for the specific experimental setup. Such criteria could be based for example on the goodness of the LDF fit. In general, it is expected that the photon-optimized LDF doesn't fit proton-induced air shower events well (see the two example events shown in Fig. 3). Hence, the goodness of the fit could in principle be used to select photon-like events and to further improve the search for UHE photons.

Acknowledgments

We would like to thank our colleagues from the Pierre Auger Collaboration for many fruitful discussions. We also thank the anonymous reviewer for his valuable comments on an earlier version of the manuscript, which helped to improve the paper. This work is supported by the German Federal Ministry of Education and Research (BMBF) and the Helmholtz Alliance for Astroparticle Physics (HAP).

References

[1] M. Risse, P. Homola, Search for ultra-high-energy photons using air showers, *Mod. Phys. Lett. A* 22 (2007) 749–766. doi:10.1142/S0217732307022864.

[2] The Pierre Auger Collaboration, Observation of the Suppression of the Flux of Cosmic Rays above 4×10^{19} eV, *Phys. Rev. Lett.* 101 (2008) 061101. doi:10.1103/PhysRevLett.101.061101.

[3] The Pierre Auger Collaboration, A targeted search for point sources of EeV photons with the Pierre Auger Observatory, *ApJL* 837 (2017) L25. doi:10.3847/2041-8213/aa61a5.

[4] F. R. Klinkhamer, Potential sensitivities to Lorentz violation from nonbirefringent modified Maxwell theory of Auger, HESS, and CTA, *Phys. Rev. D* 82 (2010) 105024. doi:10.1103/PhysRevD.82.105024.

[5] J. S. Díaz, F. R. Klinkhamer, M. Risse, Changes in extensive air showers from isotropic Lorentz violation in the photon sector, *Phys. Rev. D* 94 (2016) 085025. doi:10.1103/PhysRevD.94.085025.

[6] T. Bergmann, et al., One-dimensional hybrid approach to extensive air shower simulation, *Astropart. Phys.* 26 (2007) 420–432. doi:10.1016/j.astropartphys.2006.08.005.

[7] T. Pierog, et al., First Results of Fast One-dimensional Hybrid Simulation of EAS Using CONEX, *Nucl. Phys. Proc. Suppl.* 151 (2006) 159–162. doi:10.1016/j.nuclphysbps.2005.07.029.

[8] T. Pierog, et al., EPOS LHC: Test of collective hadronization with data measured at the CERN Large Hadron Collider, *Phys. Rev. C* 92 (2015) 034906. doi:10.1103/PhysRevC.92.034906.

[9] E.-J. Ahn, et al., Cosmic ray interaction event generator SIBYLL 2.1, *Phys. Rev. D* 80 (2009) 094003. doi:10.1103/PhysRevD.80.094003.

[10] F. Riehn, et al., A new version of the event generator Sibyll, Proc. of the 34th ICRC, The Hague, Netherlands, 2015. arXiv:1510.00568.

[11] S. Ostapchenko, Monte Carlo treatment of hadronic interactions in enhanced Pomeron scheme: QGSJET-II model, *Physical Review D* 83 (2011) 014018. doi:10.1103/PhysRevD.83.014018.

[12] The Pierre Auger Collaboration, The Pierre Auger Cosmic Ray Observatory, *Nucl. Instr. Meth. Phys. Res. A* 798 (2015) 172–213. doi:10.1016/j.nima.2015.06.058.

[13] The Telescope Array Collaboration, The surface detector array of the Telescope Array experiment, *Nucl. Instr. Meth. Phys. Res. A* 689 (2012) 87–97. doi:10.1016/j.nima.2012.05.079.

[14] The Pierre Auger Collaboration, Depth of maximum of air-shower profiles at the Pierre Auger Observatory. I. Measurements at energies above $10^{17.8}$ eV, *Phys. Rev. D* 90 (2014) 122005. doi:10.1103/PhysRevD.90.122005.

[15] The Pierre Auger Collaboration, Upper limit on the cosmic-ray photon flux above 10^{19} eV using the surface detector of the Pierre Auger Observatory, *Astropart. Phys.* 29 (2008) 243–256. doi:10.1016/j.astropartphys.2008.01.003.

[16] The Telescope Array Collaboration, Upper limit on the flux of photons with energies above 10^{19} eV using the Telescope Array surface detector, *Phys. Rev. D* 88 (2013) 112005. doi:10.1103/PhysRevD.88.112005.

[17] G. Ros, et al., A new composition-sensitive parameter for ultra-high energy cosmic rays, *Astropart. Phys.* 35 (2011) 140–151. doi:10.1016/j.astropartphys.2011.06.011.

[18] M. Settimo for the Pierre Auger Collaboration, An update on a search for ultra-high energy photons using the Pierre Auger Observatory, Proc. of the 32nd ICRC, Beijing, China, 2011. arXiv:1107.4805.

[19] The Pierre Auger Collaboration, A search for point sources of EeV photons, *Astrophys. J* 789 (2014) 160. doi:10.1088/0004-637X/789/2/160.

[20] The Pierre Auger Collaboration, Search for photons with energies above 10^{18} eV using the hybrid detector of the Pierre Auger Observatory, *JCAP* 04 (2017) 009. doi:10.1088/1475-7516/2017/04/009.

[21] G. Ros, et al., Improving photon-hadron discrimination based on cosmic ray surface detector data, *Astropart. Phys.* 47 (2013) 10–17. doi:10.1016/j.astropartphys.2013.05.014.

[22] D. Newton, J. Knapp, A. Watson, The optimum distance at which to determine the size of a giant air shower, *Astropart. Phys.* 26 (2007) 414–419. doi:10.1016/j.astropartphys.2006.08.003.

- [23] T. Pierog, et al., Dependence of the longitudinal shower profile on the characteristics of hadronic multiparticle production, Proc. of the 29th ICRC, Pune, India, 2005.
- [24] I. Valiño for the Pierre Auger Collaboration, The flux of ultra-high energy cosmic rays after ten years of operation of the Pierre Auger Observatory, Proc. of the 34th ICRC, The Hague, Netherlands, 2015. [arXiv:1509.03732](#).
- [25] D. Heck, et al., CORSIKA: A Monte Carlo Code to Simulate Extensive Air Showers, Tech. Rep. FZKA 6019, Forschungszentrum Karlsruhe (1998).
- [26] A. Ferrari, et al., FLUKA: a multi-particle transport code, Tech. Rep. CERN-2005-010, INFN-TC-2005-11, SLAC-R-773, CERN (2005). [doi:10.5170/CERN-2005-010](#).
- [27] G. Battistoni, et al., The FLUKA code: description and benchmarking, AIP Conf. Proc. 896 (2007) 31. [doi:10.1063/1.2720455](#).
- [28] S. Argiró, et al., The offline software framework of the Pierre Auger Observatory, Nucl. Instr. Meth. Phys. Res. A 580 (2007) 1485–1496. [doi:10.1016/j.nima.2007.07.010](#).
- [29] M. Kobal, A. Filipčič, D. Zavrtanik for the Pierre Auger Collaboration, Thinning of High-Energy Cosmic-Ray Air-Showers, Proc. of the 26th ICRC, Salt Lake City, USA, 1999.
- [30] M. Risse, D. Heck, J. Knapp, S. Ostapchenko, EAS Simulations at Auger Energies with CORSIKA, Proc. of the 27th ICRC, Hamburg, Germany, 2001.
- [31] P. Billoir, A sampling procedure to regenerate particles in a ground detector from a "thinned" air shower simulation output, Astropart. Phys. 30 (2008) 270–285. [doi:10.1016/j.astropartphys.2008.10.002](#).
- [32] M. De Domenico, et al., Reinterpreting the development of extensive air showers initiated by nuclei and photons, JCAP 07 (2013) 050. [doi:10.1088/1475-7516/2013/07/050](#).
- [33] B. Efron, Bootstrap methods: another look at the jackknife, Ann. Stat. 7 (1979) 1–26. [doi:10.1214/aos/1176344552](#).
- [34] R. A. Fisher, The use of multiple measurements in taxonomic problems, A. Eug. 7 (1936) 179–188. [doi:10.1111/j.1469-1809.1936.tb02137.x](#).
- [35] F. G. Schröder, Radio detection of cosmic-ray air showers and high-energy neutrinos, Prog. Part. Nucl. Phys. 93 (2017) 1–68. [doi:10.1016/j.pnpnp.2016.12.002](#).